

# A robust Bayesian methodology for damage localization in plate-like structures using ultrasonic guided-waves

Sergio Cantero-Chinchilla<sup>a,d,\*</sup>, Juan Chiachío<sup>b</sup>, Manuel Chiachío<sup>c</sup>, Dimitrios Chronopoulos<sup>a</sup>, Arthur Jones<sup>a</sup>

<sup>a</sup> Institute for Aerospace Technology & The Composites Group, The University of Nottingham, NG7 2RD, United Kingdom

<sup>b</sup> Department of Naval Architecture, Ocean & Marine Engineering, University of Strathclyde, Glasgow, G4 0LZ, United Kingdom

<sup>c</sup> Dept. Structural Mechanics & Hydraulics Engineering, University of Granada, 18001, Spain

<sup>d</sup> Aernnova Engineering Division S.A., Madrid, 28034, Spain

---

## Abstract

SHM methods for damage detection and localization in plate-like structures have typically relied on signal post-processing techniques applied to ultrasonic guided-waves. The time of flight is one of these signals features which has been extensively used by the SHM community for damage localization. One approach for obtaining the time of flight is by applying a particular time-frequency transform to capture the frequency and energy content of the wave at each instant of time. To this end, the selection of a suitable methodology for time-frequency transform among the many candidates available in the literature has typically relied on experience, or simply based on considerations about computational efficiency. In this paper, a full probabilistic method based on the Bayesian inverse problem is proposed to rigorously provide a robust estimate of the time of flight for each sensor independently. Then, the robust prediction is introduced as an input to the Bayesian inverse problem of damage localization. The results reveal that the proposed methodology is able to efficiently reconstruct the damage localization within a metallic plate without the need to assume a specific a priori time-frequency transform model.

*Keywords:* Bayesian inverse problem, Ultrasonic guided-waves, Time of flight, Damage localization, Multiple damage areas, Structural Health Monitoring

---

## 1. Introduction

Damage reconstruction and localization in plate-like structures using guided-waves based SHM have been mainly addressed using post-processing techniques applied to ultrasonic signals [1]. The exploration of large areas with a small attenuation [2] is one of the most remarkable characteristics that has led industries, such as the aerospace industry, to focus on guided-waves (e.g. the “PAMELA” system [3–5]). Other approaches that use acoustic-based SHM methods to localize damage in thin-walled structures are also available nowadays. These can be broadly classified into (1) passive sensing diagnostics (PSD) and (2) active sensing diagnostics techniques (ASD). In contrast to PSD techniques, which are based on sensors in “listening-mode” (e.g., acoustic emission) [6–12], ASD techniques for

---

\*Corresponding Author

Email address: Sergio.CanteroChinchilla1@nottingham.ac.uk (Sergio Cantero-Chinchilla)

## Nomenclature

$a, b$	scaling and time-shift factors	$\text{ToF}_M^{(a-s)}$	modeled ToF between actuator $a$ and sensor $s$
$c$	normalizing constant in Bayes' Theorem	$\mathcal{U}(\cdot, \cdot)$	uniform distribution
$D^{(k)}$	mean of the hyper-robust model for the $k$ -th sensor	$v$	mean of prior PDF of the velocity
$\hat{\mathbf{d}}^{(k)}$	set of $\hat{d}_j$ in the $k$ -th sensor	$V_{a-d}, V_{d-s}$	wave propagation velocity in paths $a-d$ and $d-s$ , respectively
$\hat{d}_j^{(k)}$	first energy peak provided by the $j$ -th TF model in the $k$ -th sensor	$w_j^{(k)}$	weight of the $j$ -th TF model class in the $k$ -th sensor used in the hyper-robust model
$\tilde{d}^{(k)}$	first energy peak measured in the $k$ -th sensor	$X(t)$	time series of the signal
$\mathbf{D}$	set of $D^{(k)}$ values for all the sensors	$X_a, Y_a$	actuator coordinates
$\mathcal{D}^{(k)}$	signal acquired in the $k$ -th sensor	$X_d, Y_d$	damage position coordinates
$e$	model error of ellipse-based ToF model	$X_s, Y_s$	sensor coordinates
$g_j(\cdot)$	$j$ -th TF model	$\alpha(t)$	magnitude of the analytic signal
$h(t)$	window function	$\gamma$	threshold parameter for AIMS algorithm
$\mathbf{m}$	model parameters of ellipse-based ToF model	$\varepsilon$	error term in TF model
$\mathcal{M}_j^{(k)}$	$j$ -th TF model class for the $k$ -th sensor	$\zeta$	number of state of the chain in M-H
$\mathbf{M}$	set of model classes $\mathcal{M}_j$	$\Theta$	set of possible values of the parameters in the BIP
$N$	number of sensors	$\theta$	set of ToF model parameters including $\sigma_e$
$N_m$	number of model classes	$\rho$	scaling factor in the prior PDF of $\sigma_e$
$N_i^A$	number of samples in $i$ -th annealing level	$\sigma_\varepsilon$	standard deviation of $\varepsilon$
$\mathcal{N}(\cdot, \cdot)$	Gaussian distribution	$\sigma_e$	standard deviation of model error of ellipse-based ToF model
$P(\cdot)$	probability	$\sigma_M$	MAP value of $\sigma_e$
$p(\cdot)$	probability density	$\sigma_v$	standard deviation of prior PDF of the velocity
$q(\cdot)$	proposal PDF in MCMC sampling algorithms	$\Psi(t)$	analyzing wavelet
$r$	acceptance rate for the M-H algorithm	$\omega_j(t)$	instantaneous frequency
$T_s$	number of samples generated in M-H algorithm		
$\text{ToF}_{\mathcal{D}}^{(a-s)}$	measured ToF between actuator $a$ and sensor $s$		

9 plate-like structures emit ultrasonic waves that interact with the structure and are measured by sensors [13]. Sparse  
 10 or phased-array sensors' layouts are placed so that the structure is actively interrogated on demand, which confers  
 11 higher accuracy and reliability [14]. Potential safety and economical implications in condition-based maintenance are  
 12 extra-motivations for the use of this SHM technique.

13 Moreover, the need for autonomous techniques that provide accurate health state indicators is specially crucial for  
 14 aerospace structures, which are based on a considerable number of critical structural components requiring frequent

15 inspection. Once a damaged area is detected, i.e. through analysis of damage tolerance exceedance, proper operational  
16 decisions can be taken. Two general approaches are typically adopted for damage detection: (1) model-based inverse  
17 problems, whereby detailed damage information (e.g. the severity of damage as residual strength) [15] can be obtained  
18 from the measured signal at a considerable computational cost; and (2) inverse problems based on post-processed  
19 signal features, whereby other relevant information, e.g. the damage position or the damage severity, can be obtained  
20 more efficiently. With regards to the second approach, several damage reconstruction techniques have been reported  
21 in the literature [2, 16–18]. Among them, the time-of-flight (ToF) has been extensively used as a signal feature for  
22 its efficiency in obtaining information about material properties along with damage localization using post-processing  
23 scattered signals.

24 Time-frequency (TF) representation techniques have been intensively used for the extraction of ToF as a signal  
25 feature. By TF representation, a frequency domain spectrum can be obtained at each instant of time [19], however the  
26 results slightly differ from each other depending on the adoption of the various approaches available in the literature.  
27 Amongst them, the Hilbert-Huang transform (HHT), the continuous wavelet transform (CWT), the short-time Fourier  
28 transform (STFT) and the Wigner-Ville distribution (WVD) [19–22], are some of the most commonly used techniques  
29 in ultrasonic guided-waves based SHM applications [23–25]. Typically, the selection of one among the available  
30 options has been based on the modeler’s experience or based on specific TF resolution characteristics. However, the  
31 selection of an unappropriated model may result in a biased damage identification [26, 27] due to the disparate model  
32 assumptions and hypotheses adopted for each of them. In other words, the choice of a particular TF approach instead  
33 of another one is subject to *epistemic* uncertainty (i.e., lack of knowledge). Moreover, ultrasound-based damage  
34 localization conveys other sources of uncertainty which are mostly related with the measurement system and physical  
35 properties of the material. They might produce unreliable damage predictions should these uncertainties are not  
36 properly considered and quantified within the calculations.

37 To partially address this modeling issue, a number of researchers have proposed the use of probability-based  
38 methods [28–30]. Among them, the Bayesian inverse problem (BIP) applied to ultrasound based damage localization  
39 is getting increasing attention within the SHM community, although it is still in its early stage. In [24], the BIP was  
40 successfully proven in localizing damage areas in aluminum plates. More recently, a BIP methodology to account  
41 for the anisotropy in the *group velocity* was proposed in [23] for composite laminates. Notwithstanding, there is  
42 still an evident need for a rigorous treatment of the uncertainty in modeling the damage localization using ultrasonic  
43 guided-waves based methods, overall when multiple damage locations are expected.

44 This paper proposes a multi-level Bayesian framework to rigorously account for the overall uncertainty in appli-  
45 cation to the problem of ultrasound-based damage localization using Lamb waves. The main novelty of this paper is  
46 that it provides a unified methodology to rationally address the problem of damage identification using ultrasounds  
47 from probabilistic Bayesian principles: first, the problem of TF model selection is addressed for a given experimental  
48 configuration based on *posterior probabilities* that assess the relative degree of belief [31] of a particular model over a  
49 set of candidates; then, the problem of damage identification and localization is carried out using a BIP based on sig-

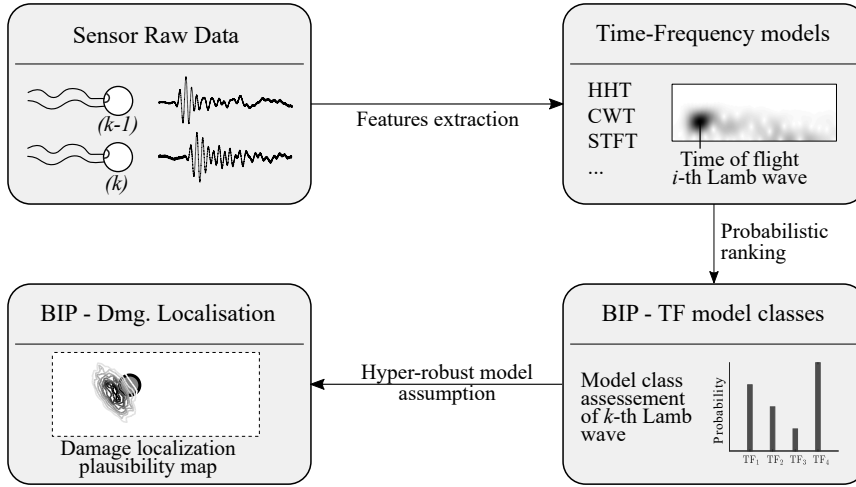


Figure 1: General workflow proposed to address the challenge of damage localization. Note that the signal data can be obtained by numerical (e.g. FEM) or experimental methods (e.g. using PZT transducers, a signal generator, and an oscilloscope) [13].

50 nal features adopting a *hyper-robust* TF model resulted from the first assessment level. To this end, once the raw data  
 51 have been acquired, two BIPs are hierarchically formulated for each piezoelectric (PZT) sensor so that the outcome  
 52 of the model selection problem is used as input for damage localization, as shown in Figure 1. In this framework,  
 53 uncertainties coming from (1) material’s mechanical properties, (2) measurement errors, and (3) epistemic uncertainty  
 54 in the TF model due to the Heisenberg principle [19, 30], are taken into account. The proposed approach relies on rig-  
 55 orous *probability-logic* assumptions for model class selection [32] and as such, it avoids experience-based decisions  
 56 about the optimal post-processing technique. Here, probability is interpreted as a multi-valued logic that expresses  
 57 the degree of belief of a proposition conditioned on the given information [32, 33]. The methodology is applied in  
 58 two case studies using aluminum plates with one and two damaged areas, respectively. For the particular problem of  
 59 damage localization, the asymptotic independent Markov sampling (AIMS) [34, 35] algorithm is adopted to solve the  
 60 resulting Bayesian inverse problem, showing high efficiency in dealing with damage multi-modality. In general, the  
 61 results show the efficiency of the proposed methodology in reconstructing the damage position in plate-like structures  
 62 using guided-waves, while rigorously accounting for the modeling uncertainties in the reconstruction.

63 The remainder of the paper is organized as follows: Section 2 shows the TF models used in the proposed model  
 64 selection problem. Section 3 comprises the probabilistic methodology used to obtain the robust estimate of the ToF  
 65 for each sensor. The BIP principles used to obtain the damage localization are presented in Section 4. In Section 5,  
 66 the proposed framework is applied in two case studies to serve as example. Section 6 discusses the robustness of the  
 67 proposed methodology. Finally, Section 7 provides concluding remarks.

## 68 2. Time-frequency models

69 Among the most used TF models in the literature, four of them are selected in this paper to be assessed and ranked  
70 using the proposed Bayesian methodology for each sensor, independently; namely the HHT, CWT, STFT, and WVD.  
71 The main formulation of these TF representation techniques is shown in the following subsections.

### 72 2.1. Hilbert-Huang transform

73 The HHT is obtained by the sum of intrinsic mode functions (IMF) whereby the spectrum is defined after per-  
74 forming the Hilber transform over each IMF component [20, 26], as follows:

$$g_1(t) = \sum_{j=1}^n \alpha_j(t) \exp\left(i \int \omega_j(t) dt\right) \quad (1)$$

75 where  $\alpha_j(t)$  is the magnitude of the analytic signal which is typically considered as the envelope of the input time  
76 series or directly the signal acquired by the sensor,  $n$  is the number of IMF components, and  $\omega_j(t)$  is the instantaneous  
77 frequency. Equation (1) represents the amplitude and instantaneous frequency as function of time.

### 78 2.2. Continuous wavelet transform

79 TF wavelets are used in the CWT to obtain the TF representation of the assessed signal, by:

$$g_2(b, a) = \frac{1}{\sqrt{a}} \int_{-\infty}^{\infty} X(t) \overline{\Psi\left(\frac{t-b}{a}\right)} dt \quad (2)$$

80 where  $X(t)$  represents the time series of the signal,  $\Psi(t)$  denotes the analysing wavelet,  $a > 0$  is the scale factor,  $b$   
81 is the time-shift variable, and the overline denotes the complex conjugate [21, 36]. Remarkable time and frequency  
82 resolution are obtained using this model.

### 83 2.3. Short-time Fourier transform

84 Alternatively, the TF representation can be obtained with a STFT, which performs Fourier transforms to a moving  
85 window in the assessed signal [19, 37], as follows:

$$g_3(\omega, t) = \frac{1}{2\pi} \int_{-\infty}^{\infty} e^{-i\omega\tau} X(\tau) h(\tau - t) d\tau \quad (3)$$

86 where  $X(t)$  is the time series,  $h(t)$  is a window function, and  $\omega$  denotes the frequency. The energy spectrum of an  
87 STFT is known as a spectrogram.

88 *2.4. Wigner-Ville distribution*

89 The WVD can be interpreted as a measure of the signal's local time-frequency energy [37], and it is defined as  
 90 follows:

$$g_4(\omega, t) = \int_{-\infty}^{\infty} X\left(t + \frac{\tau}{2}\right) \overline{X\left(t - \frac{\tau}{2}\right)} e^{-i\omega\tau} d\tau \quad (4)$$

91 where  $X(t)$  is the time series and the overline denotes the complex conjugate. This technique is highly effective in  
 92 detecting and localizing Dirac impulses and sinusoids [19, 37].

93 **3. Bayesian model class ranking**

94 The TF models in Section 2 are just different alternatives based on a number of simplifying hypotheses and  
 95 modeling assumptions to represent the same reality. Instead, for a particular model, the validity of such simplifying  
 96 assumptions depends on the adopted values of certain model parameters (e.g. the dispersion parameter). Thus, to  
 97 simultaneously identify both the plausibility of each TF model and the values of the model parameters that better suit  
 98 the information coming from the raw ultrasonic data, a Bayesian inverse problem (BIP) is proposed here. Given a  
 99 plate-like structure monitored through a set of PZT sensors, the BIP is addressed separately for each PZT sensor due  
 100 to the potential differences between sensors, such as different working environments or manufacturing defects.

101 *3.1. Stochastic embedding of TF models*

102 Let us consider a candidate TF model defined by the relationship  $g_j : \mathbb{R}^n \rightarrow \mathbb{R}$  between a discrete signal  $\mathcal{D}^{(k)} \in \mathbb{R}^n$   
 103 acting as input and the model output  $g_j \in \mathbb{R}$ , where  $k$  denotes the  $k$ -th sensor in the structure. Next, let  $\hat{d}_j^{(k)} \in \mathbb{R}$  be the  
 104 first energy peak observed in the scattered ultrasound signal, so that  $\hat{d}_j^{(k)} = g_j(\mathcal{D}^{(k)})$ . Under the assumption that  $g_j$  is  
 105 only a candidate model over a set of alternatives [32] (e.g. like those described in Section 2), then the measured first  
 106 peak, denoted here as  $\tilde{d}^{(k)}$ , would be more rigorously represented as an uncertain variable, as follows:

$$\tilde{d}^{(k)} = g_j\left(\mathcal{D}^{(k)}\right) + \varepsilon \quad (5)$$

107 where  $\varepsilon$  is an uncertain error term which accounts for the discrepancy between  $\hat{d}_j^{(k)}$  and  $\tilde{d}^{(k)}$ , namely the modeled and  
 108 measured values for the first energy peak, respectively. Following the Principle of Maximum Information Entropy  
 109 (PMIE) [32, 33], this error can be conservatively assumed to be modeled as a zero-mean Gaussian distribution with  
 110 standard deviation  $\sigma_\varepsilon$ , i.e.,  $\varepsilon \sim \mathcal{N}(0, \sigma_\varepsilon)$ . The PMIE enables a rational way to establish a probability model for the  
 111 model error term such that it produces the largest uncertainty (largest Shannon entropy); the selection of any other  
 112 probability model would lead to an unjustified reduction in such uncertainty [32]. Thus, following Equation (5), a

113 probabilistic description of the TF model can be obtained as:

$$p(\tilde{d}^{(k)} | \mathcal{M}_j^{(k)}, \sigma_\varepsilon) = (2\pi\sigma_\varepsilon^2)^{-\frac{1}{2}} \exp\left(-\frac{1}{2} \left(\frac{\tilde{d}^{(k)} - g_j^{-1}(\mathcal{D}^{(k)})}{\sigma_\varepsilon}\right)^2\right) \quad (6)$$

114 where  $\mathcal{M}_j^{(k)}$  denotes the  $j$ -th candidate *model class* within a set of  $N_m$  available TF models  
 115  $\mathbf{M} = \{\mathcal{M}_1^{(k)}, \dots, \mathcal{M}_j^{(k)}, \dots, \mathcal{M}_{N_m}^{(k)}\}$ . Each model class is defined by the stochastic TF model given by Equa-  
 116 tion (6) along with the *prior* probability density function (PDF) of the model parameter  $\sigma_\varepsilon$ ,  $p(\sigma_\varepsilon | \mathcal{M}_j^{(k)})$ . This prior  
 117 PDF represents the initial degree of belief of the values of  $\sigma_\varepsilon$  within a set of possible values  $\Theta \subseteq \mathbb{R}$  before the  
 118 information from measurements is incorporated through Bayesian updating, as explained further below. For all the  
 119 sensors in the structure, the stochastic model is defined independently, thus accounting for different potential sources  
 120 of errors and uncertainties.

### 121 3.2. Model parameters estimation

122 Previously to obtain the model parameter updating from measurements, a preliminary assessment of the influence  
 123 of the dispersion parameter  $\sigma_\varepsilon$  in the model class assessment and ranking was carried out, which showed a relatively  
 124 high sensitivity of the resulting model class assessment to the value of this parameter. Thus, a first stage of the BIP is  
 125 conceived to obtain the set of most plausible values for  $\sigma_\varepsilon$  given a set of data  $\hat{\mathbf{d}}^{(k)} = \{\hat{d}_1^{(k)}, \dots, \hat{d}_{N_m}^{(k)}\}$ , which corresponds  
 126 to a set of  $N_m$  values obtained by adopting each TF model class. To this end, the posterior PDF  $p(\sigma_\varepsilon | \hat{\mathbf{d}}^{(k)}, \mathcal{M}_j^{(k)})$  of  
 127 the dispersion parameter  $\sigma_\varepsilon$  given the  $j$ -th TF model class ( $\mathcal{M}_j^{(k)}$ ), is required. Thus, by using Bayes' theorem, this  
 128 posterior PDF is given by:

$$p(\sigma_\varepsilon | \hat{\mathbf{d}}^{(k)}, \mathcal{M}_j^{(k)}) = c^{-1} p(\hat{\mathbf{d}}^{(k)} | \sigma_\varepsilon, \mathcal{M}_j^{(k)}) p(\sigma_\varepsilon | \mathcal{M}_j^{(k)}) \quad (7)$$

129 where  $c$  is a normalizing constant, so that:

$$\int_{\Theta} p(\sigma_\varepsilon | \hat{\mathbf{d}}^{(k)}, \mathcal{M}_j^{(k)}) d\sigma_\varepsilon = \int_{\Theta} c^{-1} p(\hat{\mathbf{d}}^{(k)} | \sigma_\varepsilon, \mathcal{M}_j^{(k)}) p(\sigma_\varepsilon | \mathcal{M}_j^{(k)}) d\sigma_\varepsilon = 1 \quad (8)$$

130 In Equation (7),  $p(\hat{\mathbf{d}}^{(k)} | \sigma_\varepsilon, \mathcal{M}_j^{(k)})$  is the likelihood function, which expresses how likely the data  $\hat{\mathbf{d}}^{(k)}$  are repro-  
 131 duced by the stochastic model in Equation (6) if model class  $\mathcal{M}_j^{(k)}$  is adopted, as shown in Figure 2. This likelihood  
 132 function can be obtained by substitution of the values of  $\hat{\mathbf{d}}^{(k)}$  as the output of the stochastic model, as follows:

$$p(\hat{\mathbf{d}}^{(k)} | \sigma_\varepsilon, \mathcal{M}_j^{(k)}) = \prod_{\ell=1}^{N_m} p(\hat{d}_\ell^{(k)} | \sigma_\varepsilon, \mathcal{M}_j^{(k)}) \quad (9)$$

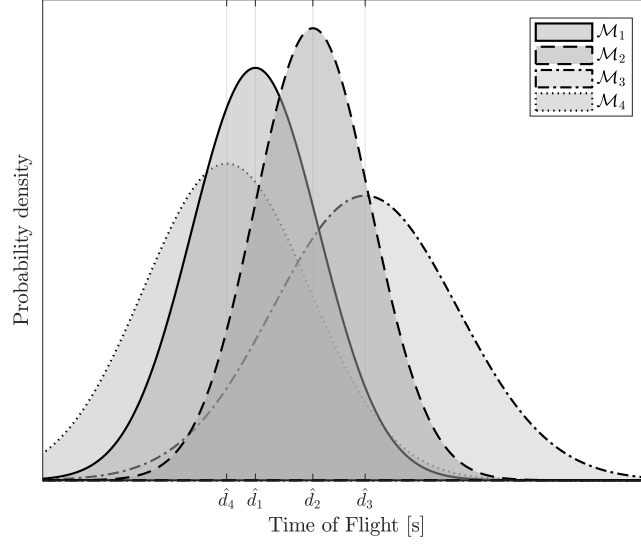


Figure 2: Likelihood functions derived from each time-of-flight ( $\hat{d}_j^{(k)}$ ). The standard deviation provided by *level I* of the proposed model ranking is expected to have different values in each model-class. The time-of-flight data are then substituted in the likelihood function  $p(\hat{\mathbf{d}}^{(k)}|\sigma_\varepsilon, \mathcal{M}_j^{(k)})$ .

133 Therefore, Equation (7) rewrites as:

$$p(\sigma_\varepsilon|\hat{\mathbf{d}}^{(k)}, \mathcal{M}_j^{(k)}) \propto \left\{ \prod_{\ell=1}^{N_m} p(\hat{d}_\ell^{(k)}|\sigma_\varepsilon, \mathcal{M}_j^{(k)}) \right\} p(\sigma_\varepsilon|\mathcal{M}_j^{(k)}) \quad (10)$$

134 Furthermore, it is observed that the evaluation of the normalizing constant  $c$  in Equation (7) cannot usually be eval-  
 135 uated analytically except for special cases based upon linear models and Gaussian uncertainties [38]. However,  
 136 stochastic simulation based on MCMC methods [39, 40] can be used to obtain samples from the posterior avoiding  
 137 the evaluation of  $c$ , as shown in the next section.

### 138 3.3. Model class assessment

139 The probabilistic approach for model class assessment is motivated by the uncertainty about the TF model based on  
 140 the assumed hypotheses and simplifications adopted for its formulation [32, 33]. Once the posterior  $p(\sigma_\varepsilon|\hat{\mathbf{d}}^{(k)}, \mathcal{M}_j^{(k)})$   
 141 is obtained, the plausibility of the model class  $\mathcal{M}_j^{(k)}$  can be obtained by applying the Total Probability Theorem as:

$$\begin{aligned} P(\mathcal{M}_j^{(k)}|\hat{\mathbf{d}}^{(k)}) &= \int_{\Theta} P(\mathcal{M}_j^{(k)}|\hat{\mathbf{d}}^{(k)}, \sigma_\varepsilon) p(\sigma_\varepsilon|\hat{\mathbf{d}}^{(k)}) d\sigma_\varepsilon = \\ &= \int_{\Theta} \frac{p(\hat{\mathbf{d}}^{(k)}|\mathcal{M}_j^{(k)}, \sigma_\varepsilon) P(\mathcal{M}_j^{(k)}|\mathbf{M})}{\sum_{\ell=1}^{N_m} p(\hat{\mathbf{d}}^{(k)}|\mathcal{M}_\ell^{(k)}, \sigma_\varepsilon) P(\mathcal{M}_\ell^{(k)}|\mathbf{M})} p(\sigma_\varepsilon|\hat{\mathbf{d}}^{(k)}) d\sigma_\varepsilon \end{aligned} \quad (11)$$

142 where  $p(\sigma_\varepsilon|\hat{\mathbf{d}}^{(k)})$  denotes the posterior PDF obtained by Equation (10). Equation (11) can be simplified by applying



143 the asymptotic Laplace's approximation [32] as follows:

$$P\left(\mathcal{M}_j^{(k)}|\hat{\mathbf{d}}^{(k)}\right) \approx \frac{p\left(\hat{\mathbf{d}}^{(k)}|\mathcal{M}_j^{(k)}, \sigma_{M_j}\right) P\left(\mathcal{M}_j^{(k)}\right)}{\sum_{\ell=1}^{N_m} p\left(\hat{\mathbf{d}}^{(k)}|\mathcal{M}_\ell^{(k)}, \sigma_{M_j}\right) P\left(\mathcal{M}_\ell^{(k)}\right)} \quad (12)$$

144 where the conditioning on  $\mathbf{M}$  has been suppressed for simplicity and  $\sigma_{M_j}$  is the maximum a posteriori (MAP) value  
 145 of the posterior PDF  $p(\sigma_\varepsilon|\hat{\mathbf{d}}^{(k)}, \mathcal{M}_j^{(k)})$ , i.e.:

$$\sigma_M = \arg \max_{\sigma_\varepsilon} p(\sigma_\varepsilon|\hat{\mathbf{d}}^{(k)}, \mathcal{M}_j^{(k)}) \quad (13)$$

### 146 3.4. Hyper-robust model estimation

147 The probability-based ranking of the model classes  $\mathcal{M}_j^{(k)}$  obtained above provides information about the degree  
 148 of belief of the  $j$ -th TF model class for each sensor. However, a *hyper-robust* model [32] is proposed to account for  
 149 the uncertainties held by all the model classes, thus providing a rigorous tool to address the model class selection. The  
 150 hyper-robust model for a specific sensor  $k$  is defined as a weighted average of each TF model as follows:

$$p\left(\tilde{d}^{(k)}|\mathbf{M}\right) = \sum_{\ell=1}^{N_m} p\left(\tilde{d}^{(k)}|\mathcal{M}_\ell^{(k)}, \sigma_{M_\ell}\right) P\left(\mathcal{M}_\ell^{(k)}|\hat{\mathbf{d}}^{(k)}\right) \cong \mathcal{N}\left(\sum_{\ell=1}^{N_m} w_\ell^{(k)} \hat{d}_\ell^{(k)}, \sum_{\ell=1}^{N_m} \left(w_\ell^{(k)} \sigma_{M_\ell}\right)^2\right) \quad (14)$$

151 where  $\tilde{d}^{(k)}$  are the possible ToF values and  $w_\ell^{(k)}$  are the weights, given by the posterior probabilities of the  $\ell$ -th  
 152 model class  $P(\mathcal{M}_\ell^{(k)}|\hat{\mathbf{d}}^{(k)})$ . Given that each stochastic model is assumed to be distributed as a Gaussian function,  
 153 a simplified expression for the hyper-robust Gaussian distribution is also provided in Equation (14). However, to  
 154 address the damage localization problem, the use of a stochastic model as the input data would require an intensively  
 155 computational effort. Instead, the mean value of the hyper-robust model in the  $k$ -th sensor, denoted as  $D^{(k)}$ , is adopted.

## 156 4. Bayesian damage localization

### 157 4.1. Probabilistic description of ToF model

158 In this section, the damage localization is addressed by a model-based BIP using an ellipse-based ToF model [28],  
 159 which has been extensively used for damage localization in guided-waves based SHM. For this problem,  $N_p$  actuator-  
 160 sensor paths are considered in a plate-like structure to excite and receive Lamb waves for damage localization by  
 161 screening changes of their ToF. To this end, the ToF information of the scattered signals can be theoretically obtained  
 162 as follows [41]:

$$\text{ToF}^{(a-s)} = \frac{\sqrt{(X_d - X_a)^2 + (Y_d - Y_a)^2}}{V_{a-d}} + \frac{\sqrt{(X_d - X_s)^2 + (Y_d - Y_s)^2}}{V_{d-s}} \quad (15)$$

163 where  $(X_d, Y_d)$  are the coordinates of the damage,  $(X_a, Y_a)$  are the actuator transducer coordinates,  $(X_s, Y_s)$  are the  
164 coordinates of one arbitrary sensor transducer, and  $V_{a-d}$  and  $V_{d-s}$  are the wave propagation velocities of the actuator-  
165 damage and damage-sensor paths respectively. These velocities are the same under the assumption of isotropic mate-  
166 rials and a concentrated damage within a bounded region, i.e.  $V = V_{a-d} = V_{d-s}$ . Alternatively, under the consideration  
167 of orthotropic materials, such as composite structures, both velocity terms would be dependent on the angle of the  
168 actuator-damage and damage-sensor paths,  $V_{a-d}(\alpha_a)$  and  $V_{d-s}(\alpha_s)$  respectively [23].

169 To probabilistically describe the ToF model given by Equation (15), uncertainties coming from the data, material  
170 properties, and also from the model itself, need to be accounted for. To this end, a set of uncertain model parameters  
171  $\mathbf{m} = \{X_d, Y_d, V\}$  are considered in this problem to describe the uncertainty about the damage coordinates as well as  
172 the wave propagation velocity. The set  $\mathbf{m}$  of model parameters is augmented with a model error term  $e \in \mathbb{R}$ , resulting  
173 in a set of model parameters defined as  $\boldsymbol{\theta} = \{\mathbf{m}, \sigma_e\} = \{X_d, Y_d, V, \sigma_e\} \in \Theta$ , where  $\sigma_e$  is the standard deviation of the  
174 error term  $e$  and  $\Theta$  is the model parameter space. This set of parameters is further updated through Bayes' Theorem,  
175 as will be explained below. The referred model error term  $e \in \mathbb{R}$  is considered to account for the non-existence of a  
176 theoretical ToF model that fully represent the reality, so that:

$$\text{ToF}_{\mathcal{D}}^{(a-s)} = \text{ToF}_M^{(a-s)}(\mathbf{m}) + e = \text{ToF}_M^{(a-s)}(\boldsymbol{\theta}) \quad (16)$$

177 where subscripts  $M$  and  $\mathcal{D}$  from  $\text{ToF}_M^{(a-s)}$  and  $\text{ToF}_{\mathcal{D}}^{(a-s)}$  refer to modeled and measured ToF, respectively. Note in  
178 Equation (16) that  $e$  provides the discrepancy between  $\text{ToF}_M^{(a-s)}$  and  $\text{ToF}_{\mathcal{D}}^{(a-s)}$  values. By the PMIE, this error term  
179 can be conservatively described as a zero-mean Gaussian distribution with covariance  $\sigma_e$  as  $\mathcal{N}(0, \sigma_e)$ . Thus, a  
180 probabilistic description of the ToF model from Equation (16) can be obtained as:

$$p\left(\text{ToF}_{\mathcal{D}}^{(a-s)} | \text{ToF}_M^{(a-s)}(\boldsymbol{\theta})\right) = (2\pi\sigma_e^2)^{-\frac{1}{2}} \exp\left(-\frac{1}{2} \left(\frac{\text{ToF}_{\mathcal{D}}^{(a-s)} - \text{ToF}_M^{(a-s)}(\boldsymbol{\theta})}{\sigma_e}\right)^2\right) \quad (17)$$

181 Observe that Equation (17) provides a measurement of the similarity of the modeled and measured ToF. Also, note  
182 that Equation (17) provides a likelihood function for the  $\text{ToF}_{\mathcal{D}}^{(a-s)}$  data under the  $\text{ToF}_M^{(a-s)}(\boldsymbol{\theta})$  model.

#### 183 4.2. Model parameter estimation

184 Given the likelihood function in Equation (17), one can obtain the posterior PDF of the model parameters given the  
185 ToF data  $\mathbf{D} = \{D^{(1)}, \dots, D^{(N)}\}$ , where  $N$  is the total number of sensors by applying the well-known Bayes' Theorem  
186 as:

$$p(\boldsymbol{\theta} | \mathbf{D}) = \frac{p(\mathbf{D} | \boldsymbol{\theta}) p(\boldsymbol{\theta})}{p(\mathbf{D})} \quad (18)$$

187 where  $p(\boldsymbol{\theta})$  is the prior PDF of the model parameters, and  $p(\mathbf{D} | \boldsymbol{\theta})$  is the likelihood function for the set of data  $\mathbf{D}$ . Given  
188 the stochastic independence of the measurements, the likelihood can be expressed as  $p(\mathbf{D} | \boldsymbol{\theta}) = \prod_{k=1}^N p(D^{(k)} | \boldsymbol{\theta})$ , where

---

**Algorithm 1** Pseudo-code implementation of AIMS algorithm.

---

- 1: **Preamble** Define  $\gamma \in \mathbb{R} \triangleright$  {threshold for the essential sampling size (ESS)},  $N_0^A, \dots, N_j^A, \dots, N_m^A \triangleright$  {total number of samples in each annealing level  $j$ },  $q_0(\cdot|\boldsymbol{\theta}), \dots, q_j(\cdot|\boldsymbol{\theta}), \dots, q_m(\cdot|\boldsymbol{\theta}) \triangleright$  {proposal distributions at each annealing level  $j$ }
  - 2: **Algorithm**
    - 3:  $j = 0 \triangleright$  {first annealing level}
    - 4: Sample  $\{\boldsymbol{\theta}_0^{(i)}\}_{i=1}^{N_0^A}$ , where  $\boldsymbol{\theta}_0^{(i)} \sim p(\boldsymbol{\theta})$
    - 5: Obtain the ESS as a measure of the similarity between  $p_0(\cdot)$  and the target distribution  $p(\cdot)$
    - 6: **while**  $\text{ESS}/N_j < \gamma$  **do**
      - 7: Obtain the normalized importance weights as a measure of the relative importance of the likelihood function in annealing levels  $j+1$  and  $j$  [34].
      - 8: Run the M-H algorithm to generate  $N$  states of a Markov chain with target distribution  $p_{j+1}(\cdot)$ : Generate a Markov chain  $\boldsymbol{\theta}_{j+1}^{(1)} \dots \boldsymbol{\theta}_{j+1}^{(N_{j+1}^A)}$  with target distribution  $p_{j+1}(\cdot)$  [34].
      - 9: Calculate the ESS as a measure of the similarity between  $p_{j+1}(\cdot)$  and the target  $p(\cdot)$
      - 10:  $j \leftarrow j+1$
    - 11: **end while**
    - 12: Set  $m = j+1 \triangleright$  {total number of steps in the annealing approach}
    - 13: Generate a Markov chain  $\boldsymbol{\theta}_m^{(1)} \dots \boldsymbol{\theta}_m^{(N_m^A)}$  with distribution  $p_m(\cdot) = p(\cdot)$  at annealing level  $m$ .
- 

189 each factor  $p(D^{(k)}|\boldsymbol{\theta})$  is given by Equation (17). Finally,  $p(\mathbf{D})$  is the evidence of the data under the model specified  
190 by  $\boldsymbol{\theta}$ . This term, which acts as a normalizing factor within the Bayes' theorem, can be bypassed through sampling,  
191 e.g. using Markov Chain Monte Carlo (MCMC) methods [42]. Thus, Equation (18) can be rewritten as:

$$p(\boldsymbol{\theta}|\mathbf{D}) \propto \left\{ \prod_{k=1}^N p(D^{(k)}|\boldsymbol{\theta}) \right\} p(\boldsymbol{\theta}) \quad (19)$$

### 192 4.3. Asymptotic independence Markov sampling algorithm

193 In practice, the presence of multiple damage locations in plate-like structures is possible, thus the updating algo-  
194 rithm used to obtain the posterior PDF of the locations of such potential damage should be able to provide samples  
195 of a multimodal PDF. In the literature, the majority of available MCMC algorithms can identify multimodal posterior  
196 PDFs at the cost of increasing the computational burden, which can be exacerbated if large dimensional parameter  
197 spaces are explored, or by introducing *ad-hoc* algorithmic modifications [43]. To overcome this drawback, the asymp-  
198 totic independence Markov sampling (AIMS) algorithm [34] is used here due to its efficiency to provide samples from  
199 multi-modal posterior PDFs. In AIMS algorithm, a posterior PDF  $p(\cdot)$  is approximated using a combination of three  
200 well-known stochastic simulation methods. To this end, *simulated annealing* is used to obtain the target distribution  
201  $p(\cdot)$  from the prior distribution by sampling intermediate distributions  $p_j(\cdot)$  through a *random walk M-H*. The inter-  
202 mediate distributions  $p_j(\cdot)$  are approximated by using *importance sampling*. A pseudo-code implementation of AIMS  
203 method is provided as Algorithm 1.

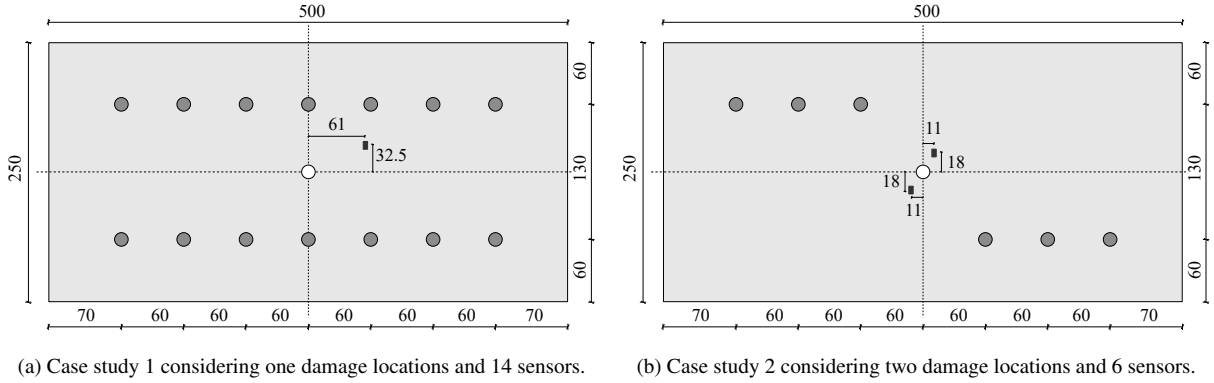


Figure 3: Representation of the aluminum plates considered in both case studies along with the position and layout of the sensors (dimensions expressed in millimetres). The white circle represents the actuator, which is positioned in the center of the plate. Damage is represented using dark rectangles.

## 204 5. Case studies

205 In this section, two case studies are presented to validate the proposed model class selection methodology using  
 206 a set of guided-waves synthetically generated by finite element modeling (FEM). The methodology is applied to two  
 207 cases of damage detection and localization considering one and two damaged areas, respectively.

### 208 5.1. Synthetic signal generation

209 To numerically generate the input signals, Lamb waves are modeled using Abaqus® for the simulations. The  
 210 waves are generated over a thin plate made of aluminum-based alloy 2024-T351 with dimensions  $0.5 \text{ m} \times 0.25 \text{ m}$ ,  
 211 as depicted in Figure 3 (see further properties about the aluminum alloy 2024-T351 in Table 1). In Figure 3 (panel  
 212 (a)), sensor numbering is established starting from S1 for the left-most upper sensor to S14 for the right-most down  
 213 sensor. In panel (b), which corresponds to the case of two damage locations, sensors are analogously arranged starting  
 214 from S1 to S6. For the ToF calculations, the Abaqus/Explicit module is used in this work for its effectiveness in  
 215 simulating the transient behavior of the ultrasonic guided-waves.

Table 1: Material and structural properties (aluminum alloy 2024-T351 [44]) used in the Abaqus model.

Young's modulus [GPa]	Poisson's ratio [-]	Density [kg/m <sup>3</sup> ]	Thickness [mm]
73.1	0.33	2780	1.5

216 A 4-node, quadrilateral, stress-displacement shell element with reduced integration and a large-strain formulation,  
 217 referred to as S4R element [45], is used for the plate model, which is uniformly meshed using square elements of  
 218 1 mm size. The element size is determined by the smallest wavelength  $\lambda_{min}$  of the guided-wave mode represented.  
 219 A minimum of 10 nodes per wavelength is normally required to ensure the avoidance of spatial aliasing [46]. The  
 220 signal excitation is modeled as a perpendicular point force generated as a sine tone-burst of 5 cycles centered at

221 a frequency  $f = 100$  kHz. This frequency is selected to avoid extra complexity in the signal post-processing due  
 222 to the appearance of possible higher order guided-waves modes. When the frequency is maintained at relatively  
 223 low values, only both anti-symmetric 0 (A0) and symmetric 0 (S0) modes are excited [46]. Given that the wave  
 224 propagation velocity of the mode<sup>1</sup> captured by the model is around  $V = 1950$  m/s, the maximum element size would  
 225 be  $\lambda/10 = (V/f)/10 = 1.95$  mm. However, note that the selected element size (1 mm) is nearly half of the maximum  
 226 value. Next, the damage is modeled as a rectangular hole of dimension 2 mm  $\times$  4 mm for both case studies considered  
 227 in this paper. Free boundary conditions are considered in both cases. The ultrasonic signals are then received by the  
 228 sensors in both undamaged and damaged cases. Afterwards, signals from both states are subtracted, thus the scattered  
 229 information from the damage is obtained, as described in Section 4.1.

### 230 5.2. Model selection results

231 As previously mentioned, the simulated response of the plate to Lamb waves is used as data within the Bayesian  
 232 framework. First, the standard deviation parameter  $\sigma_\varepsilon$  is defined as  $\sigma_\varepsilon = \rho \cdot \hat{d}_j^{(k)}$ , where  $\hat{d}_j^{(k)}$  is the time of arrival at  
 233 the  $k$ -th sensor using the  $j$ -th TF model, and  $\rho$  is a factor defined within a sufficiently large interval, which in this  
 234 example is taken as (0, 0.5]. Therefore, the prior PDF of  $\sigma_\varepsilon$  can be expressed as a uniform distribution over the  
 235 referred interval, i.e.  $p(\sigma_\varepsilon) = \mathcal{U}(0, 0.5 \cdot \hat{d}_j^{(k)})$ . The posterior PDF  $p(\sigma_\varepsilon | \hat{\mathbf{d}}^{(k)}, \mathcal{M}_j^{(k)})$  is obtained through samples using  
 236 the Metropolis-Hasting (M-H) algorithm (see a pseudo-code implementation in Appendix A) with  $T_s = 40000$  and a  
 237 Gaussian *proposal distribution*, i.e.,  $q(\theta' | \theta) = \mathcal{N}(\theta, \sigma)$ , where  $\sigma$  is the standard deviation of the M-H random walk  
 238 which is selected such that the acceptance rate  $r$  lies within the interval [0.2, 0.4] [47–49]. The maximum a posteriori  
 239 (MAP) parameter is then computed and introduced as an input for the model class selection problem, as explained in  
 240 Section 3.3.

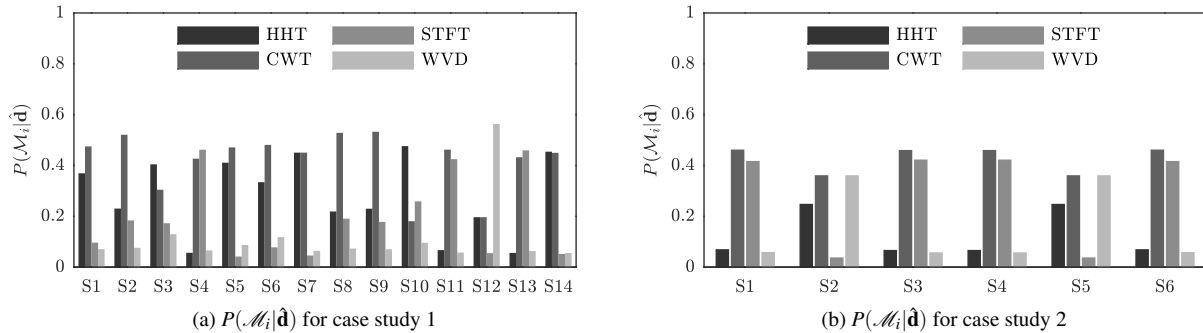


Figure 4: Posterior probability  $P(\mathcal{M}_i | \hat{\mathbf{d}})$ .

241 The resulting posterior probabilities from Equation (12) are subsequently used to rank the candidate TF models  
 242 for each of the sensors, as shown in Figures 4a and 4b for case study 1 and 2, respectively. Observe from these results

<sup>1</sup>The referred mode is the anti-symmetric mode (A0) since only the bending mode can be captured with shell elements.

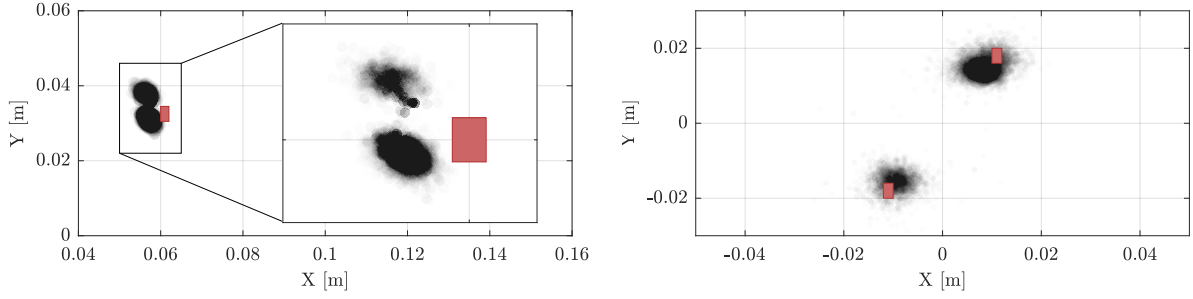
Table 2: Time of arrival ( $D^{(k)}$ ) obtained as the mean of the hyper-robust models given by Equation (14).

	Sensor	Time $D^{(k)}$ [ $\mu$ s]	Sensor	Time $D^{(k)}$ [ $\mu$ s]
Case study 1	S1	157.53	S8	163.33
	S2	125.29	S9	136.23
	S3	98.125	S10	114.66
	S4	71.539	S11	94.115
	S5	49.164	S12	83.664
	S6	70.242	S13	96.235
	S7	98.500	S14	116.35
Case study 2	S1	109.96	S4	54.577
	S2	81.214	S5	81.214
	S3	54.577	S6	109.96

243 that there is not a particularly predominating TF model for all the sensors. Nonetheless, the CWT model emerges as  
244 the most plausible one for a considerable majority of sensors, i.e., 8 out of 14 sensors for the case study 1, and 4 out  
245 of 6, for case study 2. Therefore, if a single TF model had to be selected for damage identification, a rational selection  
246 based on these results would be to choose the CWT model, since the better representation of the given data for the  
247 majority of sensors is provided by this choice. This output is in agreement with most of the authors in the literature  
248 who select CWT model to obtain the ToF from the scattered signals [23, 24]. Notwithstanding, a hyper-robust model  
249 can be obtained by applying Equation (14) using the posterior probabilities of each model class. The ToFs in this case  
250 are obtained by a model average from the probabilistic model from each sensor, as shown in Table 2. These values  
251 are subsequently used to reconstruct the damage in the BIP of damage localization, which is shown next.

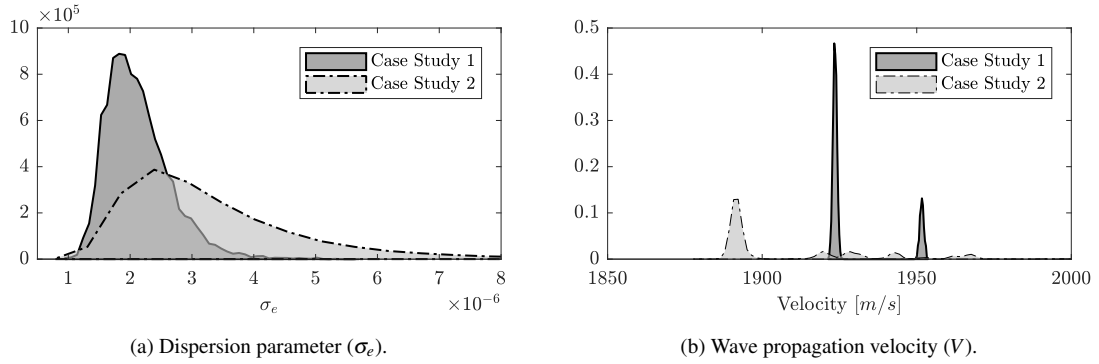
### 252 5.3. Damage localization and reconstruction

253 Once the TF models are ranked and the hyper-robust TF model is obtained, the mean values of each hyper-robust  
254 model for each sensor are used as ToF data  $\mathbf{D}$  within the BIP of damage localization, described in Section 4. The  
255 prior information of the model parameters has been defined as a uniform distribution for the damage position and  
256 dispersion parameter ( $X \sim \mathcal{U}(-0.25, 0.25)\text{m}$ ,  $Y \sim \mathcal{U}(-0.125, 0.125)\text{m}$ , and  $\sigma_e \sim \mathcal{U}(0, 10^{-4})$ ), and a Gaussian PDF  
257 for the velocity  $V \sim \mathcal{N}(v, \sigma_v)$ , where  $v = 1950\text{m/s}$  and  $\sigma_v = 40\text{m/s}$ . The posterior PDF of model parameters  $\theta$  is  
258 obtained in this case using the AIMS algorithm, with a threshold value  $\gamma = 1/2$ ,  $10^5$  samples per annealing level, and  
259 a Gaussian PDF as proposal distribution, i.e.  $q(\theta'|\theta) = \mathcal{N}(\theta, \sigma)$ , where  $\sigma$  is the standard deviation of the M-H  
260 random walk which is again selected such that the acceptance rate  $r$  lies within the interval  $[0.2, 0.4]$ . Figure 5 shows  
261 the inferred damage position for the aluminum plates of case study 1 and 2, respectively, using the hyper-robust TF  
262 model obtained by Equation (14). The hyper-robust model is obtained for each sensor by model averaging weighted  
263 using the posterior plausibilities of the TF models, showed in Figure 4. It is observed that the damage position  
264 is efficiently reconstructed with the BIP methodology presented in this paper. The results also show that for the  
265 particular case study 2, the multi-modality due to dual damage position is well addressed using the AIMS algorithm.



(a) Estimated and actual damage position ( $X - Y$ ) for the case study 1 (b) Estimated and actual damage position ( $X - Y$ ) for the case study 2

Figure 5: Damage location estimation for the plate of case study 1 and 2. The actual position of the center of the damage is depicted using red rectangles which are represented in actual dimensions.



(a) Dispersion parameter ( $\sigma_e$ ).

(b) Wave propagation velocity ( $V$ ).

Figure 6: Posterior PDFs of the  $\sigma_e$  and  $V$  parameters for both case study 1 and 2.

266 The marginal posterior distributions of the other two parameters used by the BIP of damage localization, namely  
 267 the standard deviation factor of the likelihood function  $\sigma_e$  and the wave propagation velocity  $V$ , are depicted in  
 268 Figure 6. In case study 1, a lower level of dispersion in both parameters,  $\sigma_e$  and  $V$ , is observed, whereas in case study  
 269 2, a higher dispersion is obtained.

## 270 6. Discussion

271 The proposed Bayesian methodology for damage localization has been exemplified using two case studies pre-  
 272 sented in Section 5. For each of the sensors, a Bayesian model class assessment framework is proposed to rank the  
 273 candidate TF models, according to relative plausibilities that measure the relative degree of belief of the candidate  
 274 model class in interpreting the raw signal acquired by the sensor. These relative plausibilities are then used to obtain  
 275 a hyper-robust TF model for each sensor, which provides a higher level of robustness to damage localization than just  
 276 taking the most plausible TF model among the candidate set. This robustness is clearly manifested in Figure 5a, where

277 damage position is identified in two plausible regions close to the actual damage position; an unjustified TF model  
 278 choice would lead to a biased localization due to unconsidered model uncertainty. The same behavior can be also  
 279 observed in Figure 6b for the reconstruction of the wave propagation velocity parameter. Note that the ultrasonic data  
 280 used in both case studies are synthetically obtained through FEM, although the methodology is entirely applicable to  
 281 real ultrasonic signals. However, for real ultrasonic data, the uncertainty in the damage localization would be higher  
 282 due to electronic noise or other measurement errors coming from, for instance, imperfect sensor bonding.

283 Then, a damage localization BIP using an ellipse-based model is applied to reconstruct the damage position using  
 284 the AIMS algorithm as Bayesian updating algorithm. The data  $\mathbf{D}$  are obtained by using the mean of the hyper-robust  
 285 model, given by Equation (14) for each sensor independently. The damage location has been remarkably inferred in  
 286 both case studies. However, a higher dispersion in the  $X - Y$  parameters (larger localization uncertainty) has been  
 287 found in case study 2 compared to case study 1, as can be observed in Figure 5. In addition, a higher dispersion is  
 288 identified in the marginal distribution of the standard deviation parameter  $\sigma_e$  in case study 2. This could be explained  
 289 due to the nature of the likelihood function from Equation (17), which is a Gaussian distribution. In order to properly  
 290 identify the two damage positions in this case study, the posterior values of  $\sigma_e$  (which is an updatable parameter)  
 291 need to increase, hence leading to a higher dispersion in the damage localization as well as in the velocity parameter  
 292 reconstruction, as observed in Figure 6. This points out a limitation of the proposed methodology when dealing with  
 293 multiple damage locations. In this context, a desirable further work would be the exploration of optimal likelihood  
 294 functions to deal with damage multi-modality.

295 The robustness of the proposed methodology can then be observed by comparing the Bayesian identification  
 296 results against those obtained using a deterministic approach. A well-known method to address inverse problems  
 297 efficiently, but deterministically, is by the use of genetic algorithms (GA) [50]. GA's are used to find the value of  
 298 the parameters that minimizes a *cost function*, which in this case can be defined as  $\|\text{ToF}_{\mathcal{D}}^{(a-s)} - \text{ToF}_M^{(a-s)}(\mathbf{m})\|_2^2$ , a  
 299  $L_2$ -norm of the residual time of flight between the model and the data. Figure 7 depicts the comparison between  
 300 the damage identification results obtained using the proposed Bayesian methodology and a deterministic GA-based  
 301 inverse problem. To better highlight the robustness of the proposed Bayesian damage identification methodology in the  
 302 presence of uncertainties, a bias is artificially introduced in the velocity term as a 5% of deviation in the value obtained  
 303 through Abaqus (from 1950 m/s to 1850 m/s). Note that even with this small deviation, the damage localization  
 304 results given by the GA become biased, whereas the results using Bayesian methodology are virtually immune to  
 305 such variation. This simple example demonstrates the superiority of the proposed methodology in reconstructing the  
 306 position of damage from guided-waves data, regardless of potential input errors.

307 Finally, it is worth mentioning that the position of the sensors plays a crucial role in the damage reconstruction.  
 308 As observed in Figure 3, case studies 1 and 2 have different sensor selection and layout. In this paper, a former  
 309 sensitivity study on the sensors positions was carried out to identify: (1) the best number and (2) locations of sensors  
 310 for each case study. Therefore, given the influence of the aforementioned two factors in the reconstruction of the  
 311 damage position, an immediate further work will be the exploration of an efficient methodology for optimal sensor



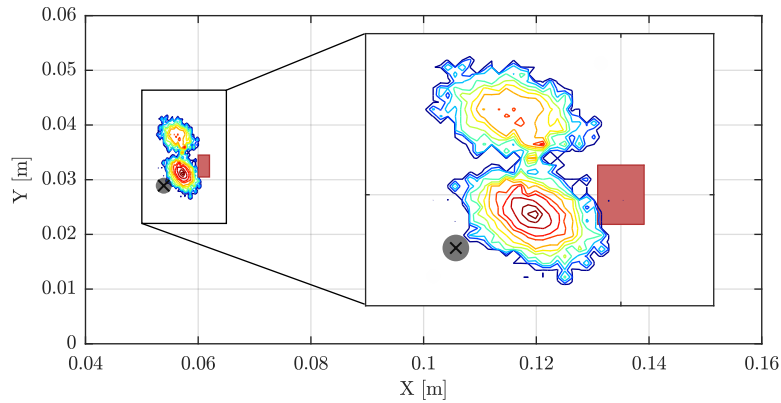


Figure 7: Comparison between a deterministic damage localization using GA (gray point) and the results obtained with the proposed Bayesian methodology.

312 configuration, based on rigorous probabilistic assumptions to deal with the aforementioned sources of uncertainties.

### 313 7. Conclusions

314 A Bayesian methodology for damage location using guided-waves is presented in this paper. This methodology  
 315 allows accounting for several sources of uncertainty, like the epistemic uncertainty due to TF model selection, and the  
 316 uncertainty coming from the measurement noise and variable material properties. The effectiveness of the method is  
 317 shown through two case studies with one and two damaged areas, respectively. The following conclusions are drawn  
 318 from this paper:

- 319 • The damage position can be accurately reconstructed using ToFs proving the effectiveness of the proposed  
 320 multi-level Bayesian inverse problem methodology;
- 321 • The use of a hyper-robust TF model as an input for the damage localization Bayesian inverse problem leads to  
 322 a more robust damage inference;
- 323 • The reconstruction of the two damage areas in case study 2 (multi-modality) has been remarkably addressed  
 324 by using the AIMS algorithm. However, under this scenario of damage, an important increase in the posterior  
 325 uncertainty of the model parameters is obtained.

326 Further research work is under consideration with regards to: (1) the assessment of a suitable likelihood function to  
 327 efficiently deal with multi-modal damage scenarios, (2) devising a rigorous technique for optimal sensor configuration  
 328 in ultrasonic guided-waves based SHM, and (3) the influence of different types of damage in the performance of the  
 329 proposed methodology.

## 330 Acknowledgements

331 This paper is part of the SAFE-FLY project that has received funding from the European Union’s Horizon 2020  
332 research and innovation programme under the Marie Skłodowska-Curie grant agreement No 721455.

## 333 Appendix A. Metropolis-Hastings simulation for Bayesian updating

334 The M-H algorithm generates samples from a specially constructed Markov chain whose stationary distribution  
335 is the required posterior PDF  $p(\boldsymbol{\theta}|\hat{\mathbf{d}}, \mathcal{M})$ . By sampling a candidate model parameter  $\boldsymbol{\theta}'$  from a *proposal distribution*  
336  $q(\boldsymbol{\theta}'|\boldsymbol{\theta}^\zeta)$ , the M-H obtains the state of the chain at  $\zeta + 1$ , given the state at  $\zeta$ , specified by  $\boldsymbol{\theta}^\zeta$ . The candidate pa-  
337 rameter  $\boldsymbol{\theta}'$  is accepted (i.e.,  $\boldsymbol{\theta}^{\zeta+1} = \boldsymbol{\theta}'$ ) with probability  $\min\{1, r\}$ , and rejected (i.e.,  $\boldsymbol{\theta}^{\zeta+1} = \boldsymbol{\theta}^\zeta$ ) with the remaining  
338 probability  $1 - \min\{1, r\}$ , where:

$$r = \frac{p(\hat{\mathbf{d}}|\boldsymbol{\theta}', \mathcal{M})p(\boldsymbol{\theta}'|\mathcal{M})q(\boldsymbol{\theta}^{\zeta-1}|\boldsymbol{\theta}')}{p(\hat{\mathbf{d}}|\boldsymbol{\theta}^{\zeta-1}, \mathcal{M})p(\boldsymbol{\theta}^{\zeta-1}|\mathcal{M})q(\boldsymbol{\theta}'|\boldsymbol{\theta}^{\zeta-1})} \quad (\text{A.1})$$

339 The process is repeated until  $T_s$  samples have been generated so that the monitored acceptance rate (ratio between  
340 accepted M-H samples over total amount of samples) reaches an asymptotic behaviour. A pseudo-code description of  
341 this method is provided below as Algorithm 2.

---

### Algorithm 2 M-H algorithm

---

1. Initialize  $\boldsymbol{\theta}^{\zeta=0}$  by sampling from the prior PDF:  $\boldsymbol{\theta}^0 \sim p(\boldsymbol{\theta}|\mathcal{M})$
  - for**  $\zeta = 1$  to  $T_s$  **do**
  2. Sample from the proposal:  $\boldsymbol{\theta}' \sim q(\boldsymbol{\theta}'|\boldsymbol{\theta}^{\zeta-1})$
  3. Compute  $r$  from Eq. A.1
  4. Generate a uniform random number:  $\alpha \sim \mathcal{U}[0, 1]$
  - if**  $r \geq \alpha$  **then**
  5. Set  $\boldsymbol{\theta}^\zeta = \boldsymbol{\theta}'$
  - else**
  6. Set  $\boldsymbol{\theta}^\zeta = \boldsymbol{\theta}^{\zeta-1}$
  - end if**
  - end for**
- 

## 342 References

- 343 [1] J. Achenbach, Wave Propagation in Elastic Solids, North-Holland Publishing Company/American Elsevier, 1973.
- 344 [2] Z. Su, L. Ye, Y. Lu, Guided Lamb waves for identification of damage in composite structures: A review, Journal of sound and vibration  
345 295 (3-5) (2006) 753–780.
- 346 [3] G. Aranguren, P. Monje, V. Cokonaj, E. Barrera, M. Ruiz, Ultrasonic wave-based structural health monitoring embedded instrument, Review  
347 of Scientific Instruments 84 (12) (2013) 125106.
- 348 [4] P. M. Monje, L. Casado, G. Aranguren, V. Cokonaj, E. Barrera, M. Ruiz, Integrated electronic system for ultrasonic structural health moni-  
349 toring, in: European workshop on structural health monitoring, 2012, pp. 1–8.
- 350 [5] A. Alcaide, E. Barrera, M. Ruiz, G. Aranguren, Damage detection on Aerospace structures using PAMELA SHM System, in: 6th International  
351 Symposium on NDT in Aerospace, Madrid, 2014.

- 352 [6] V. Giurgiutiu, Chapter 9 - Impact and Acoustic Emission Monitoring for Aerospace Composites SHM, in: V. Giurgiutiu (Ed.), Structural  
353 Health Monitoring of Aerospace Composites, Academic Press, Oxford, 2016, pp. 317 – 394.
- 354 [7] A. Tobias, Acoustic-emission source location in two dimensions by an array of three sensors, Non-destructive testing 9 (1) (1976) 9–12.
- 355 [8] J. Park, F.-K. Chang, System identification method for monitoring impact events, in: Smart Structures and Materials 2005: Smart Sensor  
356 Technology and Measurement Systems, Vol. 5758, International Society for Optics and Photonics, 2005, pp. 189–201.
- 357 [9] J. F. Markmiller, F.-K. Chang, Sensor network optimization for a passive sensing impact detection technique, Structural Health Monitoring  
358 9 (1) (2010) 25–39.
- 359 [10] L. E. Mujica, J. Vehí, W. Staszewski, K. Worden, Impact damage detection in aircraft composites using knowledge-based reasoning, Structural  
360 Health Monitoring 7 (3) (2008) 215–230.
- 361 [11] C. Hiche, C. K. Coelho, A. Chattopadhyay, A strain amplitude-based algorithm for impact localization on composite laminates, Journal of  
362 Intelligent Material Systems and Structures 22 (17) (2011) 2061–2067.
- 363 [12] H. Fu, C.-M. Vong, P.-K. Wong, Z. Yang, Fast detection of impact location using kernel extreme learning machine, Neural Computing and  
364 Applications 27 (1) (2016) 121–130.
- 365 [13] M. Mitra, S. Gopalakrishnan, Guided wave based structural health monitoring: A review, Smart Materials and Structures 25 (5) (2016)  
366 053001.
- 367 [14] L. Wang, F. Yuan, Active damage localization technique based on energy propagation of Lamb waves, Smart Structures and Systems 3 (2)  
368 (2007) 201–217.
- 369 [15] J. Chiachío, N. Bochud, M. Chiachío, S. Cantero, G. Rus, A multilevel Bayesian method for ultrasound-based damage identification in  
370 composite laminates, Mechanical Systems and Signal Processing 88 (2017) 462–477.
- 371 [16] C. H. Wang, J. T. Rose, F.-K. Chang, A synthetic time-reversal imaging method for structural health monitoring, Smart materials and structures  
372 13 (2) (2004) 415.
- 373 [17] J. E. Michaels, T. E. Michaels, Guided wave signal processing and image fusion for in situ damage localization in plates, Wave motion 44 (6)  
374 (2007) 482–492.
- 375 [18] J. E. Michaels, A. J. Croxford, P. D. Wilcox, Imaging algorithms for locating damage via in situ ultrasonic sensors, in: Sensors Applications  
376 Symposium, 2008. SAS 2008. IEEE, IEEE, 2008, pp. 63–67.
- 377 [19] L. Cohen, Time-frequency Analysis: Theory and Applications, Prentice-Hall, Inc., Upper Saddle River, NJ, USA, 1995.
- 378 [20] N. E. Huang, Z. Shen, S. R. Long, M. C. Wu, H. H. Shih, Q. Zheng, N.-C. Yen, C. C. Tung, H. H. Liu, The empirical mode decomposition and  
379 the Hilbert spectrum for nonlinear and non-stationary time series analysis, in: Proceedings of the Royal Society of London A: mathematical,  
380 physical and engineering sciences, Vol. 454, The Royal Society, 1998, pp. 903–995.
- 381 [21] C. K. Chui, An Introduction to Wavelets, Academic Press Professional, Inc., San Diego, CA, USA, 1992.
- 382 [22] C. Bao, H. Hao, Z.-X. Li, X. Zhu, Time-varying system identification using a newly improved HHT algorithm, Computers & Structures  
383 87 (23-24) (2009) 1611–1623.
- 384 [23] C. Fendzi, N. Mechbal, M. Rebillat, M. Guskov, G. Cofignal, A general Bayesian framework for ellipse-based and hyperbola-based damage  
385 localization in anisotropic composite plates, Journal of Intelligent Material Systems and Structures 27 (3) (2016) 350–374.
- 386 [24] G. Yan, A Bayesian approach for damage localization in plate-like structures using Lamb waves, Smart Materials and Structures 22 (3) (2013)  
387 035012.
- 388 [25] M. S. Salmanpour, Z. Sharif Khodaei, M. Aliabadi, Impact damage localisation with piezoelectric sensors under operational and environmen-  
389 tal conditions, Sensors 17 (5) (2017) 1178.
- 390 [26] B. Xu, L. Yu, V. Giurgiutiu, Advanced methods for time-of-flight estimation with application to lamb wave structural health monitoring, in:  
391 Proc. International Workshop on SHM, 2009, pp. 1202–1209.
- 392 [27] L. Peralta, X. Cai, P. Laugier, Q. Grimal, A critical assessment of the in-vitro measurement of cortical bone stiffness with ultrasound,  
393 Ultrasonics 80 (2017) 119–126.
- 394 [28] E. B. Flynn, M. D. Todd, P. D. Wilcox, B. W. Drinkwater, A. J. Croxford, Maximum-likelihood estimation of damage location in guided-wave

- 395 structural health monitoring, in: Proceedings of the Royal Society of London A: Mathematical, Physical and Engineering Sciences, Vol. 467,  
396 The Royal Society, 2011, pp. 2575–2596.
- 397 [29] L. Yu, Z. Su, Application of kernel density estimation in Lamb wave-based damage detection, *Mathematical problems in engineering* 2012.
- 398 [30] E. D. Niri, S. Salamone, A probabilistic framework for acoustic emission source localization in plate-like structures, *Smart Materials and*  
399 *Structures* 21 (3) (2012) 035009.
- 400 [31] G. Rus, J. Chiachío, M. Chiachío, Logical inference for inverse problems, *Inverse Problems in Science and Engineering* 24 (3) (2016)  
401 448–464.
- 402 [32] J. L. Beck, Bayesian system identification based on probability logic, *Structural Control and Health Monitoring* 17 (7) (2010) 825–847.
- 403 [33] E. T. Jaynes, Information theory and statistical mechanics, *Physical review* 106 (4) (1957) 620.
- 404 [34] J. L. Beck, K. M. Zuev, Asymptotically independent Markov sampling: a new Markov chain Monte Carlo scheme for Bayesian inference,  
405 *International Journal for Uncertainty Quantification* 3 (5) (2013).
- 406 [35] K. M. Zuev, J. L. Beck, Global optimization using the asymptotically independent Markov sampling method, *Computers & Structures* 126  
407 (2013) 107–119.
- 408 [36] H. Jeong, Y.-S. Jang, Wavelet analysis of plate wave propagation in composite laminates, *Composite Structures* 49 (4) (2000) 443–450.
- 409 [37] M. Niethammer, L. J. Jacobs, J. Qu, J. Jarzynski, Time-frequency representations of Lamb waves, *The Journal of the Acoustical Society of*  
410 *America* 109 (5) (2001) 1841–1847.
- 411 [38] M. S. Arulampalam, S. Maskell, N. Gordon, T. Clapp, A tutorial on particle filters for online nonlinear/non-Gaussian Bayesian tracking,  
412 *IEEE Transactions on signal processing* 50 (2) (2002) 174–188.
- 413 [39] N. Metropolis, A. W. Rosenbluth, M. N. Rosenbluth, A. H. Teller, E. Teller, Equation of state calculations by fast computing machines, *The*  
414 *journal of chemical physics* 21 (6) (1953) 1087–1092.
- 415 [40] W. K. Hastings, Monte Carlo sampling methods using Markov chains and their applications, *Biometrika* 57 (1) (1970) 97–109.
- 416 [41] J.-B. Ihn, F.-K. Chang, Pitch-catch active sensing methods in structural health monitoring for aircraft structures, *Structural Health Monitoring*  
417 7 (1) (2008) 5–19.
- 418 [42] F. Liang, C. Liu, J. Chuanhai, *Advanced Markov Chain Monte Carlo Methods*, Wiley Online Library, 2010.
- 419 [43] J. Besag, P. J. Green, Spatial statistics and Bayesian computation, *Journal of the Royal Statistical Society. Series B (Methodological)* (1993)  
420 25–37.
- 421 [44] T. Dursun, C. Soutis, Recent developments in advanced aircraft aluminium alloys, *Materials & Design (1980-2015)* 56 (2014) 862–871.
- 422 [45] ABAQUS, *Abaqus Documentation*, Dassault Systèmes, Providence, RI, USA (2016).
- 423 [46] D. Alleyne, P. Cawley, A two-dimensional Fourier transform method for the measurement of propagating multimode signals, *The Journal of*  
424 *the Acoustical Society of America* 89 (3) (1991) 1159–1168.
- 425 [47] M. Chiachío, J. Chiachío, G. Rus, J. L. Beck, Predicting fatigue damage in composites: A Bayesian framework, *Structural Safety* 51 (2014)  
426 57 – 68.
- 427 [48] A. Gelman, G. Roberts, W. Gilks, Efficient Metropolis jumping rules, *Bayesian Statistics* 5 (1996) 599–608.
- 428 [49] G. Roberts, J. Rosenthal, Optimal scaling for various Metropolis-Hastings algorithms, *Statistical Science* 16 (4) (2001) 351–367.
- 429 [50] M. Gen, R. Cheng, *Genetic algorithms and engineering optimization*, Vol. 7, John Wiley & Sons, 2000.